ADVANCED OPTICAL MATERIALS
www.advopticalmat.de

Read on Demand Images in Laser-Written Polymerizable Liquid Crystal Devices

Chloe C. Tartan, John J. Sandford O'Neill, Patrick S. Salter, Jure Aplinc, Martin J. Booth, Miha Ravnik,* Stephen M. Morris,* and Steve J. Elston**

Two-photon laser writing is a powerful technique for creating intricate, high resolution features in polymerizable materials. Here, using a single-step process to microfabricate polymer inclusions, the ability to generate read-on-demand images and identification codes in a liquid crystal (LC) device is demonstrated. These micrometer-sized polymer features are encoded directly into LC devices using direct laser writing, which locks-in the local molecular orientation at the moment of fabrication. By reading the devices with the same voltage amplitude that is used to write the polymer structures, features can be made to disappear as the director profile becomes homogeneous with the surrounding regions, effectively cloaking the structure for both polarized and unpolarized light. It is shown how this process can be used to create micrometer-scale reconfigurable emoticons and quick-response codes within a fully assembled LC device, with potential use in authenticity and identification applications.

Refractive index matching of polymer binders with liquid crystalline materials has been explored in considerable depth over many years, particularly in the context of polymer dispersed liquid crystals (LCs), where the mismatch between the refractive indices of the polymer and the LC lead to scattering of light, which can be "turned-off" by matching the refractive indices of the two separate elements using an applied voltage.[1–12] Advanced fabrication techniques such as direct laser writing (DLW)[13–15] offer new ways with which to manipulate the interplay between the refractive indices of the polymer network/binder and the LC components. In this work, we harness DLW to approach the process of refractive index matching from a slightly different perspective, by generating polymer microstructures embedded directly within a switchable LC device. By applying a varying voltage across the device, it is possible to bring the LC layer into harmony with the boundary conditions imposed by the fabricated polymer features to give a uniform refractive index profile, thereby removing scattering and masking the object in the presence of both polarized and unpolarized light.

By laser writing the polymer structures directly inside an addressable LC device, we can control the orientation of the LC molecules (described by a unit vector known as the director) during fabrication.[16] The photocured polymer retains the orientational order of the LC at the point of exposure to the ultrafast laser beam,[16–18] leading to features that are both birefringent and that dictate the local alignment of the neighboring uncured bulk of the LC. This in turn provides access to a unique set of director profiles that can be frozen-in by the DLW process than would otherwise be possible using only the alignment layers at the substrate surfaces, or other advanced 2D alignment techniques.[19–34]

An illustration of the fabrication of the polymer structures in the LC devices and the proposed concept is presented in **Figure 1**a (see the Experimental Section). The devices, which were 20 μm thick glass cells with planar surface alignment layers and transparent electrodes, contained a reactive mesogen and photoinitiator mixture that had been dispersed into the nematic LC host, E7 (Synthon), at a concentration of 30 wt% (see the Experimental Section for further details). After the glass devices had been filled, they were then exposed to bursts of tightly focused ultrashort laser pulses (see the Experimental Section and Figure S1 of the Supporting Information for an illustration of the experimental setup). In the absence of an applied voltage, the nematic LC assumes a planar-alignment, as illustrated by the results from the simulation of the director profile shown in Figure 1b (the Experimental Section and the Supporting Information). When the focused ultrafast laser is incident on the device, two-photon absorption by the photoinitiator triggers cross-linking of the reactive mesogen resulting in the creation of a pillar structure of dense polymer network that locks-in the voltage-dependent LC director profile at the

C. C. Tartan, J. J. Sandford O'Neill, Dr. P. S. Salter, Prof. M. J. Booth, Dr. S. M. Morris, Prof. S. J. Elston
Department of Engineering Science
University of Oxford
Oxford OX1 3PJ, UK
E-mail: patrick.salter@eng.ox.ac.uk; stephen.morris@eng.ox.ac.uk; steve.elston@eng.ox.ac.uk
J. Aplinc, Prof. M. Ravnik
Faculty of Mathematics and Physics
University of Ljubljana
Jadranska 19, 1000 Ljubljana, Slovenia
E-mail: miha.ravnik@fmf.uni-lj.si
Prof. M. Ravnik
Jozef Stefan Institute
Jamova 39, 1000 Ljubljana, Slovenia
The ORCID identification number(s) for the author(s) of this article can be found under https://doi.org/10.1002/adom.201800515.

DOI: 10.1002/adom.201800515

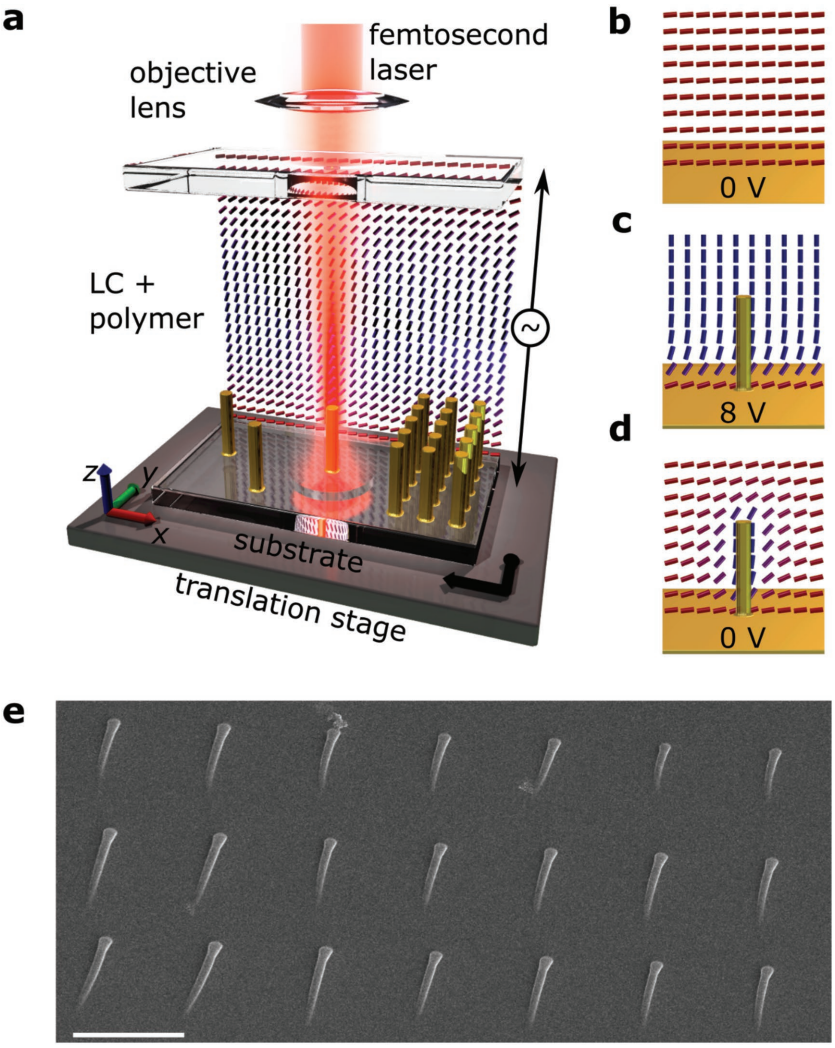

Figure 1. Direct laser writing of birefringent polymer objects in a polymerizable liquid crystal (LC) device. a) Illustration of the direct laser writing process in a LC device. b) Simulated director profile of the nematic LC device without a polymer pillar structure in the absence of an applied voltage. c) Simulated director profile when a polymer pillar is written in the device under an applied write voltage of $V_w = 8$ V and d) following the removal of the applied voltage. e) An SEM image of an array of polymer pillars. Scale bar is 40 µm.

moment of exposure to the laser beam (see Figure 1c). This voltage-driven director profile defines the alignment of the LC molecules at the surfaces of the polymer pillar irrespective of the voltage that is applied after fabrication.

The "recorded" director field is confined solely to the regions of the developed polymer that lie within the focal volume of the writing laser. The unpolymerized surrounding bulk material remains free to realign in the presence of an applied voltage post-fabrication, while the alignment within and at the surface of the pillars is fixed, as conditioned by the strong surface anchoring. This behavior is illustrated in the director simulations in Figure 1d, which shows the resultant director field when the device subsequently relaxes back to its equilibrium ground state upon removal of the applied voltage. Different LC alignments can then be "frozen-in" to the pillars by electrically switching the device to different voltage amplitudes during the laser writing procedure. The laser-written polymer pillars have dimensions ≈1 µm in diameter and ≈5 µm in height, as revealed by the scanning electron micrograph in Figure 1e, in good accordance with the expected voxel size from the focusing of the ultrafast laser beam. Since the polymer pillars preserve the orientational order of the LC molecules at the point of fabrication, they are not only birefringent in the absence of an applied voltage, but they also influence the alignment of the neighboring LC molecules in the surrounding unpolymerized regions (as indicated by the simulations in Figure 1).

To demonstrate the ability to match the refractive indices and hide the polymer pillar under specific voltage conditions, **Figure 2** shows the experimental and simulation results for a polymer pillar that has been written at a voltage of $V_w = 4$ V and is subsequently read at six different applied voltages after fabrication. As can be seen in Figure 2a, for voltages where $V_r \neq V_w$ the structures are clearly visible against the background LC phase. At these voltages, the birefringence of the polymer pillar is different from the surrounding regions of LC, which in turn leads to differences in the phase of light transmitted through the device and the features are thus distinguishable against the LC background. Conversely, when the read voltage, V_r, applied to the device matches the write voltage, V_w, (in this case $V_r = V_w = 4$ V), the director field in the regions surrounding the pillars and within the pillars themselves merge almost seamlessly into the background, thereby resulting in the object being hidden. It should be noted that for our selection of the LC device geometry and writing voltage of $V_w = 4$ V, the contrast between the polymer pillar and the unpolymerized LC is more significant at low voltages because the elastic distortion around the pillars becomes pronounced at values of $V_r < 4$ V, where the predominantly planar LC alignment in the bulk is more distinct relative to the hybrid alignment "locked-in" at the surface of the polymer pillar.

The experimental results are found to be in good agreement with simulated optical polarizing microscope images of the polymer pillars (Figure 2b). The simulations assumed a nematic LC that is subjected to planar alignment layers on the substrate surfaces and strong anchoring at the pillar surfaces commensurate with the director alignment at the moment of polymerization. The simulated optical polarizing microscope images were obtained from the calculations of the director profiles (shown in Figure 2c) using the 2 × 2 Jones matrix (the Experimental Section). The simulated microscope images in Figure 2b are in good qualitative agreement with the experimental results, confirming our hypothesis regarding the pillar

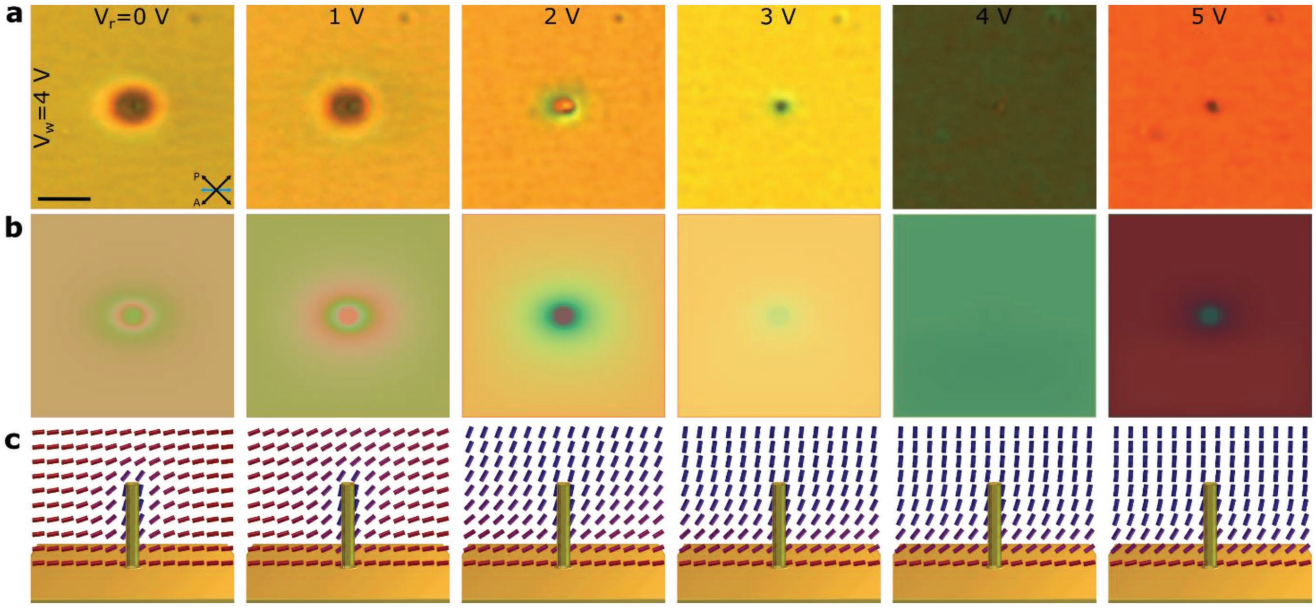

Figure 2. Voltage-induced refractive index matching of a polymer object in a liquid crystal material. a) Polarizing Optical Microscope images of a single polymer pillar fabricated at a write voltage of $V_w = 4$ V and subsequently imaged at six different read voltages ($V_r = 0$–5 V). The orientation of the crossed polarizers and the optic axis of the nematic phase are indicated by the black and blue arrows, respectively. Scale bar is 10 µm. b) Simulated optical polarizing images for the same voltages presented in (a) showing the pillar becoming "hidden" at a read voltage of 4 V and c) the associated simulated director profiles. The results highlight the effective homogeneity in the director alignment when the read and write voltages are equivalent ($V_r = V_w$).

structure and interaction with the bulk and the vanishing of the polymer pillar. The corresponding director profile simulations presented in Figure 2c show that when the polymer pillar is formed at a fabrication voltage of $V_w = 4$ V, the anchoring at the pillar surface assumes a tilted orientation in the LC director, but is planar at the substrates, leading to elastic distortion when $V_r \neq V_w$. Furthermore, the distortion in the director profile is only lifted when the read voltage (V_r) is equivalent to the write voltage (V_w), which leads to a uniform birefringence across the device, thereby cloaking the fabricated polymer features.

From a practical perspective, making the structures vanish in both polarized and unpolarized light would be highly desirable. **Figure 3** demonstrates the concept in a polymer pillar array at read voltages of 0–5 V for both polarized (Figure 3a) and unpolarized (Figure 3b) light. Each column of pillars in the array, starting from left to right, has been written at different voltages ranging from 0 to 5 V in 1 V steps. Image analysis was performed (see the Experimental Section) to quantify the visibility of the pillars for both crossed polarizers (Figure 3c) and unpolarized (Figure 3d) light and shows that the structures are not visible when $V_w = V_r$. The colormaps in the figure plot the standard deviation of each image in the matrix of grayscale images that has been created by cropping pillars from the top row of the pillar array at each read voltage. A low standard deviation (shown in black) corresponds to low visibility and a high standard deviation (white in the colormap charts) corresponds to high visibility. We therefore infer that there is a clear minimum in visibility along the diagonal line where $V_w = V_r$. Furthermore, the colormaps show the significant impact of the Fréedericksz threshold ($V_{th} \approx 0.9$ V, which is estimated based on the host LC material parameters[35]) on the visibility of the pillars, especially for unpolarized light where the pillars written above the threshold voltage ($V_w > V_{th}$) all have a similar visibility when the read voltage is also above this threshold ($V_r > V_{th}$) (and vice versa for pillars written below the threshold). Additional experimental and simulated polarizing microscope images are presented in Figure S2 of the Supporting Information for a 5 × 6 array of pillars that further demonstrate that the pillars in each column vanish when the $V_r = V_w$ condition is satisfied. This is because the surrounding director field matches the director profile that is imposed by the anchoring at the surface of the polymer pillar.

By tailoring the write and read voltages, we have shown that it is possible to make polymer objects appear and disappear in the LC host. Using this approach, it is also possible to reconfigure the structures so that different features or patterns emerge at different voltage amplitudes. **Figure 4** shows examples of patterns/images that illustrate this approach. The first is a configuration of pillars that represent a "quick-response" (QR) code (Figure 4a). By writing the pillars in the absence of an applied voltage, the QR code only becomes readable when a voltage is subsequently applied to "read" the device, unlike a previously reported polymer-stabilized cholesteric liquid crystal QR code.[36] The design of the QR code is shown in Figure S3 of the Supporting Information. We also show how features can be written at two different voltages, with a simple checkerboard design where one set of squares was written at $V_w = 0$ V and the other set of squares was written at $V_w = 5$ V (Figure 4b,d). At a read voltage of $V_r = 2.5$ V both sets of squares are visible, but at either $V_r = 0$ V or 5 V, one set of features disappears.

Taking this principle further, we have created a "microbicycle," by writing the spokes of the wheels as a line of polymer pillars at different voltages ranging from $V_w = 2$–4.5 V, while the frame was written as a continuous polymer line at $V_w = 0$ V

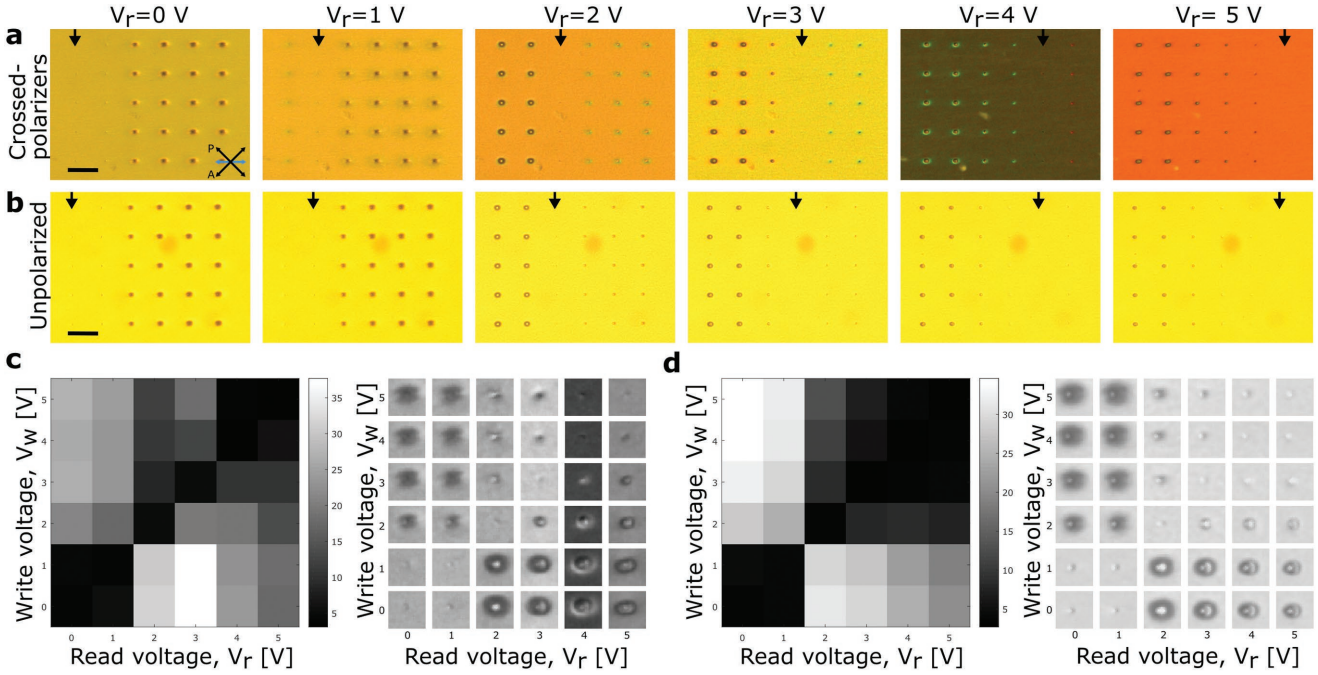

Figure 3. Refractive index matching and the cloaking of polymer structures for both polarized and unpolarized light. Optical polarizing microscope images of a 5 × 6 array of polymer pillars with a 40 µm lattice spacing for a) crossed polarizers and b) unpolarized light. The same read and write voltages were used as those presented in this figure. The orientation of the crossed polarizers and the optic axis of the nematic phase are indicated by the black and blue arrows in (a), respectively. Scale bar is 40 µm. c) Colormap chart summarizing the results of an image analysis of the polymer pillar arrays for polarized light. Individual pillars from the images were cropped and placed in a matrix according to their read and write voltage. The standard deviation of each image was evaluated to quantify the degree of visibility and plotted in the colormap chart. A minimum in visibility is present along the diagonal where $V_w = V_r$, satisfying the condition for refractive index matching. d) Colormap chart showing the corresponding image analysis for unpolarized light.

(Figure 4e). Figure 4c shows this "microbicycle" at a read voltage of V_r = 4 V, where the spoke written at V_w = 4 V disappears. Further images highlighting the reconfigurable nature of the bicycle are presented in Figure S4 of the Supporting Information along with an animation of the voltage-induced changes in the bicycle (Movie S5, Supporting Information) and a video showing the fabrication process (Movie S6, Supporting Information). Figure 4f, on the other hand, depicts a reconfigurable emoticon; by encoding different features at different voltages and then tuning the voltage to a desired setting, it is possible to view emoticons displaying a variety of expressions (the design and corresponding voltage amplitudes are presented in Figure S7, Supporting Information). In the final example (Figure 4g), we show an arrangement of polymer pillars that results in an image of the New College Crest, Oxford, which was written under a fixed voltage of V_w = 4 V; the crest appears invisible when this same voltage amplitude is applied to read the device. Here it can be seen that the crest disappears entirely when $V_r = V_w$ = 4 V.

In conclusion, a novel approach to refractive index matching has been demonstrated in polymerizable LC cells, whereby polymer structures can be made to disappear with the application of a voltage that matches the voltage applied during the fabrication procedure, resulting in an undistorted director profile between the bulk alignment of the LC and the surface anchoring conditions imposed by the polymer structures. The resultant homogeneity in the alignment reduces the elastic distortion around the polymer network to match the birefringence between the polymer and the bulk LC, such that the pillars are no longer clearly visible. We have shown that applying different voltages during fabrication of polymer objects in a photopolymerizable LC device causes the polymer network to "memorize" the local orientation of the director at the precise moment of laser writing, allowing different patterns to be encoded within the device at different voltage amplitudes. We envisage that this approach could be potentially important in the fabrication of high-value covert security features that confirm the authenticity of a consumer product, helping to combat counterfeiting and fraud.

Experimental Section

Preparation of Polymerizable Liquid Crystal Mixture: The mixture comprised of the nematic liquid crystal mixture E7 (70.7 wt%), reactive mesogen RM257 (Merck) (28.5 wt%), and Irgacure 819 (Merck) (0.8 wt%). Chemical structures of RM257 and Irgacure 819 are shown in Figure S8 of the Supporting Information. The mixture was capillary filled in the isotropic liquid phase into a liquid crystal cell manufactured by Instec Inc. The cell comprised two parallel glass plates which were coated with the transparent conductive oxide, indium tin oxide (ITO), and a rubbed polyimide alignment layer. The rubbing directions of the glass slides were antiparallel and separated by a 20 µm gap with the aid of spacer beads. After cooling to room temperature (25 °C), the LC device was mounted onto the translation stage stack in the direct laser writing system and connected to a waveform generator so that an electric field could be applied to the device during fabrication.

Direct Laser Writing: Femtosecond laser pulses of duration 100 fs from a Spectra-Physics Mai-Tai titanium-sapphire oscillator emitting at 790 nm

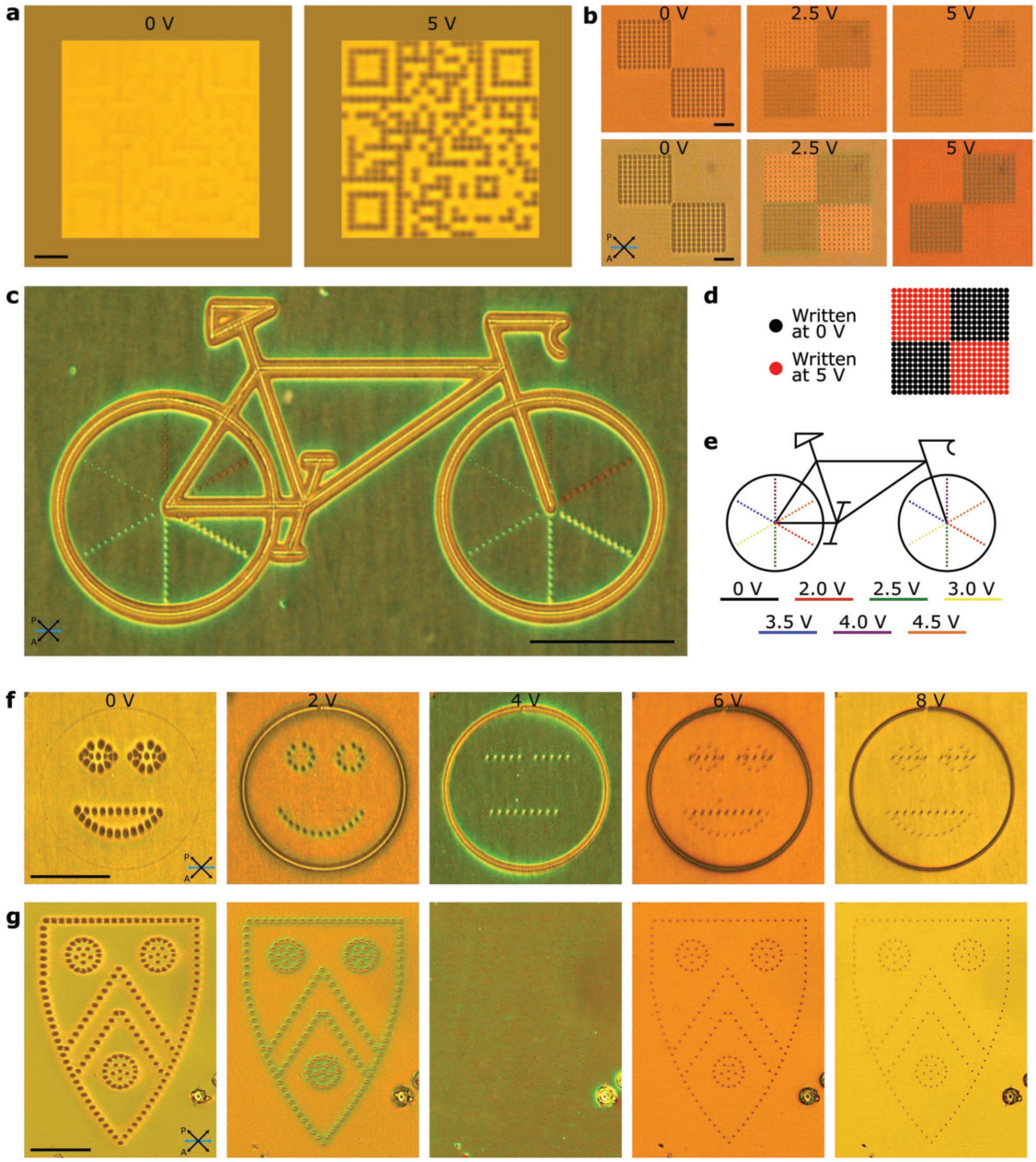

Figure 4. Reconfigurable optical elements in a polymerizable liquid crystal device. a) Image of a quick-response (QR) code written at $V_w = 0$ V with a pillar spacing of 3 µm. The code can be scanned with a smart phone only when a voltage is applied to the LC device. Scale bar is 15 µm. b) A checkerboard made from polymer pillars written at both $V_w = 0$ V and 5 V. Top row: unpolarized light. Bottom row: polarized light with a crossed polarizer configuration. Scale bar is 40 µm. d) Schematic of the checkerboard design. c) "Microbicycle" comprising of polymer walls. Image taken at $V_r = 4$ V. Scale bar is 100 µm. e) Schematic showing the voltages used to write the features in the microbicycle. f) A reconfigurable emoticon: the pillars in the outline of the face are written at $V_w = 0$ V at a spacing of 3 µm. Both the outline of the eyes and mouth were written at a write voltage of $V_w = 4$ at a spacing of 10 µm. Changes in the facial expression can be seen at different values of the applied read voltage, V_r. Scale bar is 100 µm. g) Hiding the Oxford University New College crest: the structure was written at $V_w = 4$ V and images are shown for the same read voltages as the reconfigurable emoticon. Scale bar is 100 µm. A 20 micrometer spacer bead can also be seen in the bottom right of the images. In all optical polarizing microscopy images the orientation of the crossed polarizers and the optic axis of the nematic phase are indicated by the black and blue arrows, respectively.

with a repetition rate of 80 MHz were focused with a 0.3 NA objective lens into the LC layer. The power of the fabrication laser prior to the objective was 24 mW. A Hamamatsu X10468-02 phase-only spatial light modulator was imaged onto the pupil plane of the objective lens in a 4f configuration to correct for spherical aberrations introduced when focusing inside the LC device. Liquid crystal devices were mounted onto a stack of high-resolution translation stages that allowed the sample to be moved relative to the laser focus with high precision. A red LED was used to provide transmission illumination of the device so that the fabrication could be monitored in-situ with a monochrome CCD without interfering with the photocuring process. Each polymer pillar was fabricated with a 60 ms exposure to the laser. Polymer lines were fabricated by moving the sample under continuous exposure to the pulsed laser beam.

Optical and Scanning Electron Microscopy (SEM) Characterization: An Olympus BX51 optical polarizing microscope was used to obtain images of the polymer inclusions between crossed polarizers and for unpolarized light. A long-pass filter with a cut-off wavelength of 550 nm was inserted into the optical path below the sample to ensure the microscope bulb did not cause further polymerization of any of the remaining uncured reactive mesogens in the LC mixture. The LC director (optic axis) was oriented at 45° to the polarizer and analyzer by rotating the sample until the bright state was found.

SEM was employed to confirm the dimensions of the pillar structures that consisted of the laser-written polymer network. Devices were immersed in a bath of acetone for 24 h in order to remove the unreacted liquid crystalline material. The substrate and the superstrate were then disassembled and coated in a 27.5 nm thick gold layer for SEM imaging using a secondary electron detector. A 20 kV electron beam voltage was used at a working distance of 11.5 mm.

Image Analysis: Image analysis was performed in MATLAB by first cropping an image of each pillar at each read voltage. Images of the individual pillars were extracted from the images of the pillar arrays. The images were then converted from RGB to grayscale before the standard deviation was determined. The standard deviation data was then converted to a matrix and plotted in a chart with a grayscale colormap, such that low values of standard deviation are denoted by the black squares and high values of standard deviation are represented by the white squares.

Simulations: The simulation of the nematic LC ordering in the planar-aligned cell containing polymer pillars relies upon a continuum model that uses the Landau-de Gennes free-energy minimization approach. A tensor order parameter Q_{ij} describes the orientational order of the LC molecules, while the tensorial invariants of Q_{ij} constitute the total free energy, including both the bulk and the surface free-energies to account for the anchoring on both the glass cell surfaces and the polymer pillar/bulk LC interface. The free-energy was minimized numerically using an explicit Euler relaxation finite difference scheme. Numerical simulations were performed in two consecutive stages in order to mimic the laser writing process of "locking-in" spatially dependent director fields and creating arbitrarily complex anchoring within the bulk of the device. For the first stage of the process, the nematic profile was calculated in a planar-aligned nematic cell without the presence of the polymeric structure and at an applied (writing) voltage. For the second stage, the full geometry of the cell with the pillar structures included was then simulated, where the calculated nematic profile from the first stage was used as the surface-imposed alignment direction at the pillar walls and as the fixed bulk birefringent profile within the pillars. Optical polarization microscope images were calculated by using a standard Jones 2×2 matrix formalism for the color spectrum as used in the experiments.

Supporting Information

Supporting Information is available from the Wiley Online Library or from the author.

Acknowledgements

C.C.T., J.J.S.O., P.S.S., and J.A. contributed equally to this work. C.C.T., J.J.S.O., P.S.S., M.J.B., S.M.M, and S.J.E. would like to thank the Engineering Physical Sciences Research Council UK (EP/L505584/1 and EP/N509711/1), Merck Chemicals Ltd., The Royal Society, The John Fell Fund (Oxford), and The Leverhulme Trust for financial support. J.A. and M.R. acknowledge support from the Slovenian Research Agency Grant (Grant Nos. J1-7300, L1-8135, and P1-0099) and US Air Force Office of Scientific Research, European Office of Aerospace Research and Development (Grant No. FA9550-15-1-0418, and Contract No. 15IOE028). C.C.T. would like to thank Serena Bolis, Paul Giraud, and Simon Copar for fruitful discussions and J.J.S.O would like to thank Ellis Parry, David Hansford, and Dr. Julian Fells for fruitful discussions regarding the image analysis.

Conflict of Interest

The authors declare no conflict of interest.

Keywords

laser writing, nematic liquid crystals, polymer structures, QR codes

Received: April 19, 2018
Revised: June 15, 2018
Published online:

[1] A. Mertelj, L. Spindler, M. Čopič, *Phys. Rev. E* **1997**, *56*, 549.
[2] K. Amundson, *Phys. Rev. E* **1996**, *53*, 2412.
[3] L. Bouteiller, P. Lebarny, *Liq. Cryst.* **1996**, *21*, 157.
[4] H. G. Craighead, J. Cheng, S. Hackwood, *Appl. Phys. Lett.* **1982**, *40*, 22.
[5] K. Amundson, A. van Blaaderen, P. Wiltzius, *Phys. Rev. E* **1997**, *55*, 1646.
[6] J. W. Doane, N. A. Vaz, B. G. Wu, S. Žumer, *Appl. Phys. Lett.* **1986**, *48*, 269.
[7] R. Ondris-Crawford, E. P. Boyko, B. G. Wagner, J. H. Erdmann, S. Žumer, J. W. Doane, *J. Appl. Phys.* **1991**, *69*, 6380.
[8] P. S. Drzaic, *Liq. Cryst.* **1988**, *3*, 1543.
[9] D. Coates, *J. Mater. Chem.* **1995**, *5*, 2063.
[10] D. A. Higgins, *Adv. Mater.* **2000**, *12*, 251.
[11] S. C. Jain, D. K. Rout, *J. Appl. Phys.* **1991**, *70*, 6988.
[12] P. S. Drzaic, *J. Appl. Phys.* **1986**, *60*, 2142.
[13] M. S. Rill, C. Plet, M. Thiel, I. Staude, G. Von Freymann, S. Linden, M. Wegener, *Nat. Mater.* **2008**, *7*, 543.
[14] T. Bückmann, N. Stenger, M. Kadic, J. Kaschke, A. Frölich, T. Kennerknecht, C. Eberl, M. Thiel, M. Wegener, *Adv. Mater.* **2012**, *24*, 2710.
[15] Z. Gan, Y. Cao, R. A. Evans, M. Gu, *Nat. Commun.* **2013**, *4*, 1.
[16] C. C. Tartan, P. S. Salter, T. D. Wilkinson, M. J. Booth, S. M. Morris, S. J. Elston, *RSC Adv.* **2017**, *7*, 507.
[17] H. Zeng, D. Martella, P. Wasylczyk, G. Cerretti, J. C. G. Lavocat, C. H. Ho, C. Parmeggiani, D. S. Wiersma, *Adv. Mater.* **2014**, *26*, 2319.
[18] D. J. Broer, J. Boven, G. N. Mol, G. Challa, *Makromol. Chemie* **1989**, *190*, 2255.
[19] K.-H. Chang, C. Zhang, S. Song, L.-C. Chien, *J. Appl. Phys.* **2017**, *121*, 114901.
[20] T. Guin, B. A. Kowalski, R. Rao, A. D. Auguste, C. A. Grabowski, P. F. Lloyd, V. P. Tondiglia, B. Maruyama, R. A. Vaia, T. J. White, *ACS Appl. Mater. Interfaces* **2018**, *10*, 1187.
[21] J. Kim, Y. Li, M. N. Miskiewicz, C. Oh, M. W. Kudenov, M. J. Escuti, *Optica* **2015**, *2*, 958.
[22] C. Peng, Y. Guo, T. Turiv, M. Jiang, Q.-H. Wei, O. D. Lavrentovich, *Adv. Mater.* **2017**, *29*, 1606112.
[23] L. Wang, Q. Li, *Adv. Funct. Mater.* **2016**, *26*, 10.
[24] A. Honglawan, D. A. Beller, M. Cavallaro, R. D. Kamien, K. J. Stebe, S. Yang, *Adv. Mater.* **2011**, *23*, 5519.
[25] A. J. Hess, Q. Liu, I. I. Smalyukh, *Appl. Phys. Lett.* **2015**, *107*, 071906.
[26] A. Martinez, H. C. Mireles, I. I. Smalyukh, *Proc. Natl. Acad. Sci. USA* **2011**, *108*, 20891.

[27] M. E. McConney, A. Martinez, V. P. Tondiglia, K. M. Lee, D. Langley, I. I. Smalyukh, T. J. White, *Adv. Mater.* **2013**, *25*, 5880.
[28] D. Matsunaga, T. Tamaki, H. Akiyama, K. Ichimura, *Adv. Mater.* **2002**, *14*, 1477.
[29] S. Slussarenko, A. Murauski, T. Du, V. Chigrinov, L. Marrucci, E. Santamato, *Opt. Express* **2011**, *19*, 4085.
[30] J. Y. L. Ho, V. G. Chigrinov, H. S. Kwok, *Appl. Phys. Lett.* **2007**, *90*, 243506.
[31] L. T. de Haan, C. Sánchez-Somolinos, C. M. W. Bastiaansen, A. P. H. J. Schenning, D. J. Broer, *Angew. Chem., Int. Ed.* **2012**, *51*, 12469.
[32] O. Yaroshchuk, Y. Reznikov, *J. Mater. Chem.* **2012**, *22*, 286.
[33] K. Ichimura, *Chem. Rev.* **2000**, *100*, 1847.
[34] D. Franklin, Y. Chen, A. Vazquez-Guardado, S. Modak, J. Boroumand, D. Xu, S. T. Wu, D. Chanda, *Nat. Commun.* **2015**, *6*, 1.
[35] H. L. Ong, M. Schadt, I. F. Chang, *Mol. Cryst. Liq. Cryst.* **1986**, *132*, 45.
[36] W.-S. Li, Y. Shen, Z.-J. Chen, Q. Cui, S.-S. Li, L.-J. Chen, *Appl. Opt.* **2017**, *56*, 601.